Sensors & Actuators: B. Chemical 281 (2019) 751–756

Contents lists available at ScienceDirect

Sensors and Actuators B: Chemical

journal homepage: www.elsevier.com/locate/snb

Towards an on-chip optical microsystem for spectroscopic detection of gastrointestinal dysplasia

S. Pimenta[a], S. Cardoso[b], E.M.S. Castanheira[c], G. Minas[a,*]

[a] Microelectromechanical Systems Research Unit (CMEMS - UMinho), University of Minho, Campus de Azurém, Guimarães, Portugal
[b] INESC Microsistemas e Nanotecnologias (INESC-MN) and Physics Department, Instituto Superior Técnico - Universidade de Lisboa, Lisboa, Portugal
[c] Centre of Physics (CFUM), University of Minho, Campus de Gualtar, Braga, Portugal

ARTICLE INFO

Keywords:
CMOS optical microsystem
Optical filters
Diffuse reflectance
Fluorescence
Gastrointestinal dysplasia

ABSTRACT

This paper presents a CMOS optical microsystem with a 4 × 4 photodiodes array and their readout electronics, based on 16 light-to-frequency converters, and 16 high selective optical filters, for spectrophotometric measurement of diffuse reflectance and fluorescence signals, applied to the detection of gastrointestinal dysplasia. The photodiodes array is based on n+/p-epilayer junction silicon photodiodes. Their readout electronics outputs a digital signal, with a frequency proportional to the photodiode current, featuring a sensitivity of 26 Hz/nA at 550 nm, a spectral resolution of 9 MHz and a power consumption of 1 mW. The optical filters are based on 16 thin-film narrow-band *Fabry-Perot* resonators, in which dielectric mirrors are used. They feature high transmittances and low full-width-half-maximum. Experimental measurements, using phantoms representative of the main absorbing, scattering and fluorescence properties of gastrointestinal tissues, proved the viability of the CMOS optical microsystem with the optical filters to extract those signals, when comparing the obtained results with commercial equipment. The implemented apparatus is ready to be used as a portable system on a surgery room to verify the total removing of gastrointestinal cancer tissue. Moreover, the developed approach is a step forward in the implementation of a gastrointestinal dysplasia detection miniaturized tool.

1. Introduction

Cancer is a leading cause of death in the world, comprising 8.8 million deaths in 2015, including GI (gastrointestinal) cancers (approximately 1.8 million deaths), specifically stomach, colorectal and esophageal cancers [1,2].

The detection of GI cancer in the dysplastic or pre-cancerous stage is crucial, since it gives a higher effective treatment chance to the patient. However, early stages of cancer are difficult to detect taking into account the standard visual inspection techniques, such as endoscopy and colonoscopy. This fact is due to the lack of gross morphological easily visible changes on the tissues in the dysplastic stage [2–7]. Several biopsies are performed in an attempt to increase the detection probability of those invisible lesions. However, biopsies are invasive, suffer from undersampling and their results are not immediately available, which may cause stress to the patient. As a result, it is truly important to develop minimally invasive methods/systems to guide the physicians to the biopsy sites (sites that have a higher probability to be abnormal), or even replace biopsies in the detection of GI dysplasia [2–4,7].

Diffuse reflectance and fluorescence spectroscopies have high sensitivity to some cancer biomarkers present on the tissues. Thus, small morphological and biochemical changes on these tissues, due to dysplasia, will affect the spectral signals of diffuse reflectance and fluorescence. As a result, the signals shape and intensity will be different when compared with the signals from a normal tissue. Moreover, the analysis of the spectroscopic signals with well-developed models allows the extraction of quantitative information that can improve the detection of cancer, which is not the case with other image-enhanced technologies used for detection of gastrointestinal cancers, such as NBI (narrow-band imaging) [2–12].

Several research teams have developed studies and/or systems for spectroscopy signals extraction and detection of GI cancers. In spite of some advances, most of the studies use complex and bulky components based on Xe lamps, lasers, monochromators, optical fibers and high quantum efficiency detectors. Other authors tried to miniaturize their systems, including LEDs (light emitting diodes) and photodiodes. However, none of them proposed the implementation of an on-chip optical microsystem, with all the optical detectors and their readout electronics integrated in a single chip, for extraction of diffuse reflectance and fluorescence signals [2–5,13–17]. As a result, the

* Corresponding author.
E-mail address: gminas@dei.uminho.pt (G. Minas).

https://doi.org/10.1016/j.snb.2018.10.142
Received 5 May 2018; Received in revised form 26 September 2018; Accepted 27 October 2018
Available online 29 October 2018
0925-4005/

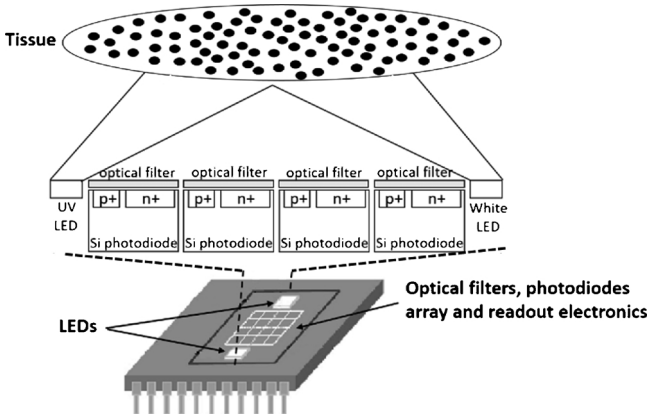

Fig. 1. Schematic of the on-chip optical microsystem for spectroscopic signals extraction (not scaled).

development of an on-chip optical microsystem, without sophisticated and complex equipment, that can be used *in-loco*, will have a high clinical value [6]. The first application of this microsystem will be its use as a portable system in a surgery room, for inspecting total removing of cancerous tissue during surgery. Another application could be its future integration with the conventional endoscopic or colonoscopic equipment, to be used by the pathologists to mark possible biopsy sites or even detect early GI cancer stages, helping in the therapeutic monitoring [2,7].

This paper describes a combined effort to implement a compact on-chip optical microsystem (Fig. 1), comprising: 16 high selective optical filters developed for selection of the spectroscopic signals in 16 relevant spectral bands, previously validated by Pimenta et al. [7], and a 4 × 4 CMOS photodiodes array (one for each optical filter) and their respective readout electronics, based on the implementation of 16 light-tofrequency (LF) converters (previously theoretical described by Correia et al. [18]). This kind of optical scheme advantages less fabrication complexity for the needed 16 spectral bands in the 350–750 nm range, when compared with other compact wavelength detectors systems such as using a Linear Vertical Filter (LVF) proposed by Schmidt et al. [19] and recently by Wan et al. [20]. The novelty presented is this paper relies on the experimental diffuse reflectance and fluorescence measurements, performed with all the above optical components assembled on-chip, which proves that the implemented apparatus (optical setup) is suitable for the first application described above: a portable system to be used on a surgery room.

2. Materials and methods

2.1. Phantoms for the experimental measurements

The used phantoms represent the main absorbing, scattering and fluorescence properties of the GI tissues, which will affect the diffuse reflectance and fluorescence signals. They were prepared containing hemoglobin (*H0267* from *Sigma-Aldrich*), 1 µm polystyrene beads (07310 from *Polysciences*), the fluorophores NADH (reduced form of nicotinamide adenine dinucleotide, *N6005* from *Sigma-Aldrich*) and Carbostyril 124 (7-amino-4-methyl-2(1*H*)-quinolinone, 363308 from *Sigma-Aldrich*), and water. Hemoglobin is the main absorber component in tissues, polystyrene represents the scattering from collagen fibers and Carbostyril 124 is a hidroxyquinoline derivative that represents the emission from collagen. Tables 1 and 2 describe the quantitative composition of those phantoms.

2.2. Optical filters

The 16 optical filters were fabricated at INESC-MN by IBD (Ion Beam Deposition, Nordiko3000 tool), on a borosilicate glass substrate. Their characterization and viability to extract spectroscopic signals, using commercial equipment, were described in our previous work [7]. Briefly, they are composed of 11 layers of MgO/TiO_2 or SiO_2/TiO_2 thin-films that form a *Fabry-Perot* resonator. Each optical filter is sensitive in a single spectral band centered at 354, 368, 387, 397, 419, 458, 485, 516, 548, 561, 582, 603, 607, 649, 701 and 746 nm, with peak transmittances ranging from 50% to 90% approximately, and a full-width-half-maximum (FWHM) averaging from 11 nm to 20 nm.

Table 1
Composition of the phantoms for diffuse reflectance experimental measurements.

Phantoms	Hemoglobin (mg/mL)	Polystyrene beads (%)	NADH (µg/mL)	Carbostyril 124 (µg/mL)
(a)	0.25	0.50	0.50	1.50
(b)	0.50	0.25	1.00	1.00
(c)	1.00	0.15	1.50	0.50
(d)	1.20	0.08	1.50	0.50

Table 2
Composition of the phantoms for fluorescence experimental measurements.

Phantoms	Hemoglobin (mg/mL)	Polystyrene beads (%)	NADH (µg/mL)	Carbostyril 124 (µg/mL)
(a)	0.25	0.50	25	75
(b)	0.25	0.50	50	150
(c)	0.25	0.50	75	225
(d)	0.25	0.50	100	300

2.3. CMOS optical microsystem

The CMOS optical microsystem, including the 4 × 4 photodiodes array (n+/p-epilayer type) and their readout electronics, was fabricated in a standard n-well 0.7 µm CMOS process using *AMIS Technology* from *Europractice*. Each photodiode has its own LF converter for fast conversion. The main features of the LF converter and its suitability for this application were already described in previous work [18], where it was fabricated and tested its preliminary version. Based on the obtained results it was implemented this new version, where it was included the 4 × 4 photodiodes array and all the control electronics. The total area of this new implemented CMOS die is 5 mm^2. Each photodiode has an active area of 100 µm × 100 µm and each LF has an area of 250 µm × 70 µm. Fig. 2 shows the new CMOS optical microsystem.

2.4. Apparatus for the CMOS optical microsystem characterization

One of the n+/p-epilayer photodiodes with an active area of 100 µm × 100 µm is assessable at the chip pinout, which makes possible its spectral characterization (responsivity), using as reference a commercial photodiode (*Hamamatsu S1336-5BQ*). For the spectral characterization, an optical setup was used (Fig. 3A and Figure S1 in Supplementary Information), comprising a quartz tungsten halogen lamp (*Newport 6334NS*) at 200 W, a picoammeter to measure the photodiodes current (*Keithley 487*), a monochromator (*Newport* 74125), an optical fiber to direct the light to the photodiodes (*Newport* 77563) and, finally, the implemented CMOS die and the commercial photodiode used as reference. In the characterization, this commercial photodiode has a 100 µm diameter pinhole on its top, which guarantees the same optical power for all the photodiodes, ensuring the accuracy of the obtained results.

The LF converter linearity was also experimentally evaluated directing a variable intensity monochromatic light source to the same n+/p-epilayer photodiode and measuring the LF converter output frequency. The lamp was powered up at 200 W, 160 W, 120 W, 80 W and

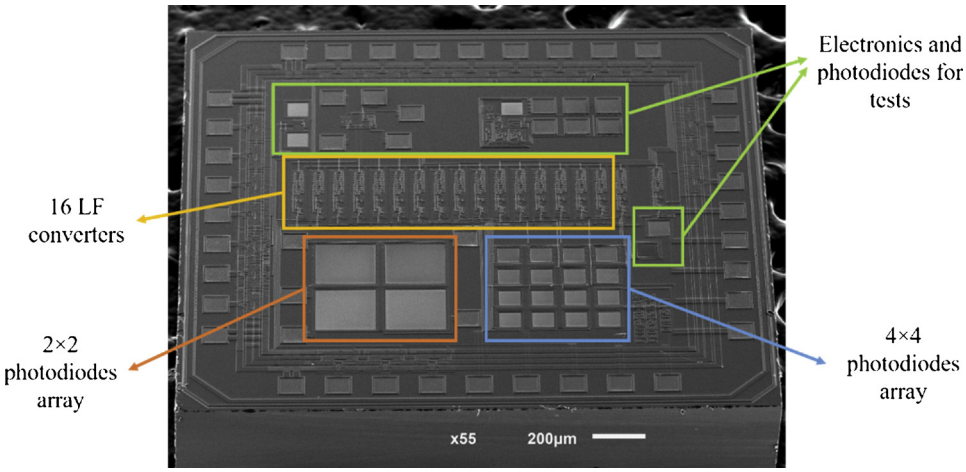

Fig. 2. SEM image (45° tilt) of the implemented CMOS optical microsystem (acquired with a JEOL JSM-6010LV SEM instrument). Each photodiode of the 4 × 4 array has an active area of 100 μm × 100 μm and each photodiode of the 2 × 2 array has an active area of 250 μm × 250 μm (an extra array added on the CMOS die, useful for tests).

40 W A DC power supply (*Mastech HY3005D-3*) at 3.5 V and a microcontroller (*stm32vl discovery*) were included in the described setup for the acquisition of LF converter output frequency (Fig. 3A grey shadow). Finally, the LF converter performance was also studied, using a current source at its input. Besides the picoammeter to measure the input current, the DC power supply at 3.5 V and the microcontroller (to acquire the low output frequencies, less than 70 kHz), the used setup included a voltage source with a resistance to produce the input current (*Keithley 6487*) and an oscilloscope (*LeCroy 9310*) to measure the output frequency of the LF converter (for high frequencies, higher than 300 kHz).

2.5. Apparatus for diffuse reflectance and fluorescence experimental measurements

The diffuse reflectance experimental measurements were carried out using the implemented CMOS optical microsystem, the fabricated optical filters and a white light (from a light source, intensity curve on Figure S2 and optical setup schematically presented on Fig. 3B and on Figure S6 of Supplementary Information). Each of the 16 fabricated optical filters was used together with one or two commercial optical filters, in order to eliminate second order effects. Transmittance spectra are shown on section A3 of Supplementary Information (Figures S3 to S5).

The fluorescence experimental measurements were performed with an optical setup (schematically presented on Fig. 3B and on Figure S7 of Supplementary Information) similar to the one used for diffuse reflectance measurements, but with the light source fixed at 350 nm, allowing excitation of the fluorophores (NADH and Carbostyril 124). Moreover, only 12 of the fabricated optical filters (with the respective commercial optical filters to eliminate second order effects) were used (between 368 nm and 607 nm), since this range is representative of the fluorescence emission properties of the fluorophores. It is important to note that the fluorescence signals emitted by the diffuse reflectance phantoms (Table 1) were too low (current intensities lower than 0.01 nA). Since the optical setup could not be improved because of the optical elements used, phantoms with higher concentration of fluorophores were considered (Table 2).

3. Results and discussion

3.1. CMOS optical microsystem characterization

Fig. 4A shows the responsivity of the CMOS n+/p-epilayer photodiode. The responsivity curve exhibits some fluctuations, introduced by the first and the second dielectric layers present above the photodiode pn-junction (in compliance with the standard rules of that CMOS technology). However, for the reported application, these wavelength dependencies will not affect the spectroscopic measurements (diffuse reflectance and fluorescence), because diffuse reflectance measurements are relative measurements (consider a reference for 100% reflectance) and the fluorescence spectral shape is not affected by these fluctuations (as seen in Section 3.3).

Fig. 4B–D present the frequency as a function of photodiode current

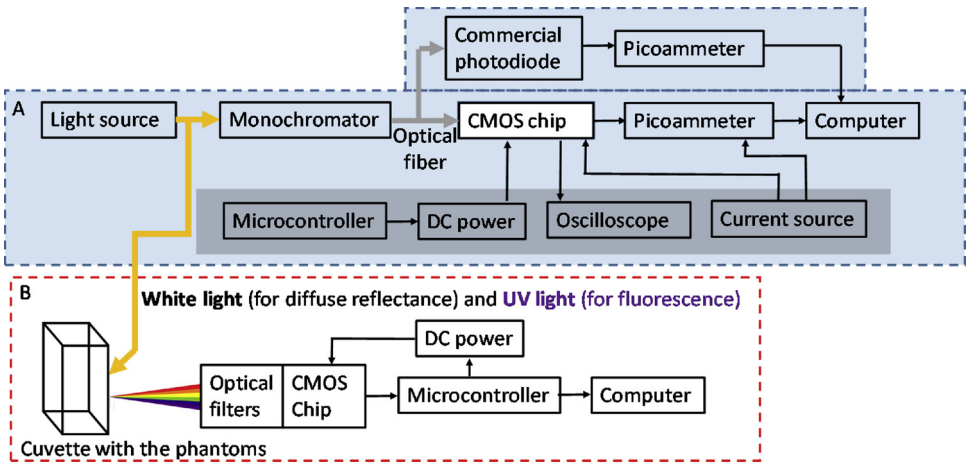

Fig. 3. Schematic of the experimental setup used for all the measurements. A) Configuration used for the CMOS optical microsystem characterization. B) Configuration used for the diffuse reflectance and fluorescence experimental measurements.

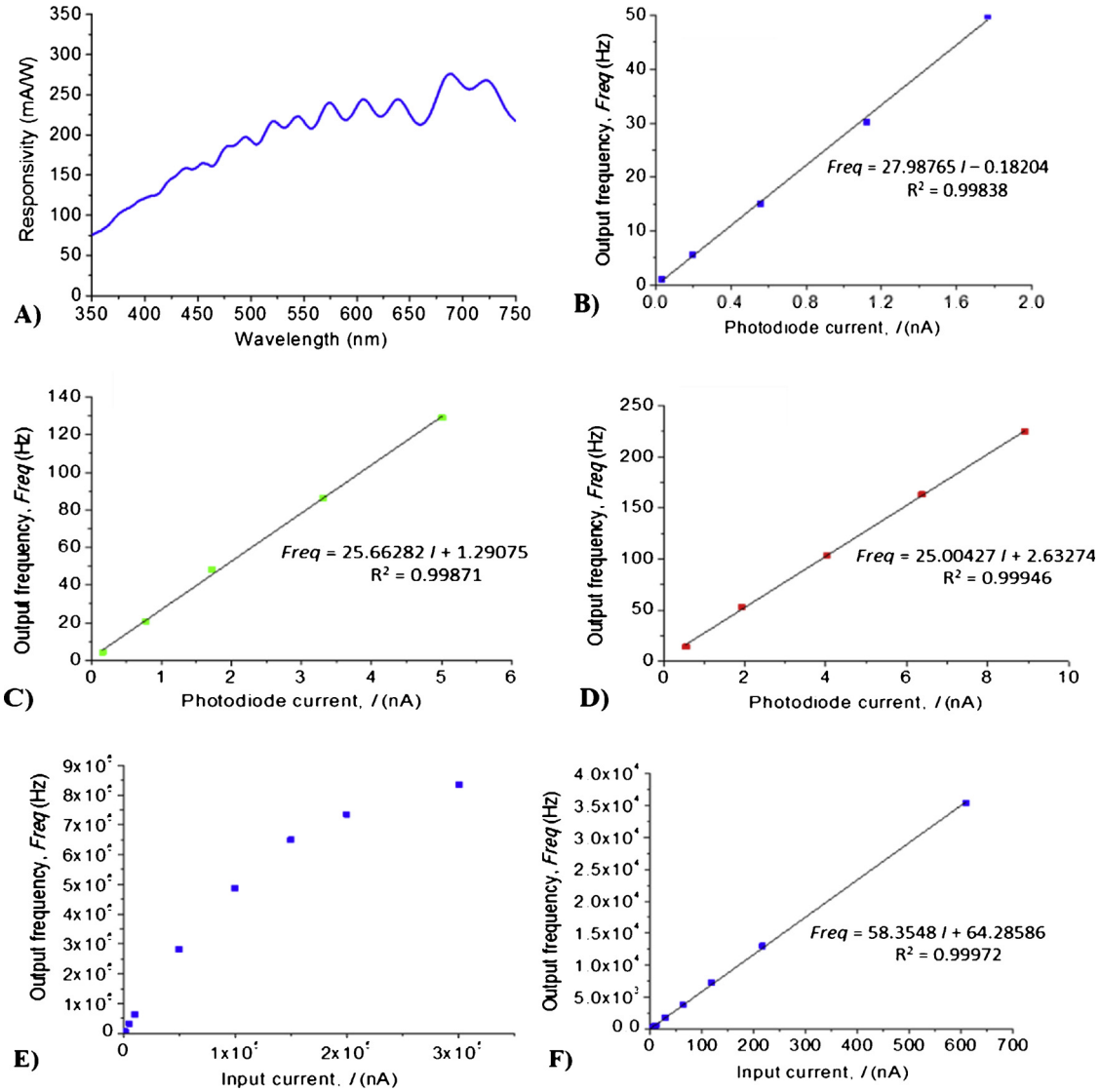

Fig. 4. A) Responsivity curve of the CMOS n+/p-epilayer photodiode. Frequency as a function of photodiode current for three fixed wavelengths: B) 450 nm, C) 550 nm and D) 700 nm. E) Measured frequency of the LF converter as a function of input current. F) Zoom showing the output frequency of the LF converter as a function of input currents up to 600 nA.

for three fixed wavelengths (450, 550 and 700 nm), covering all the desired spectral range. The results show that the output frequencies are proportional to the light intensity that reaches the photodiode, showing a good linearity, as the R^2 values are higher than 0.99. Moreover, they also show the expected wavelength dependency of the silicon (higher wavelengths, higher photodiode currents and higher frequencies), in compliance with the responsivity measurements (Fig. 4A). The measured values in absence of light were approximately 0.6 Hz for a current of 23.4 pA (dark current).

Fig. 4E exhibits the output frequencies of the LF converter for different input currents (between 60 pA and 300 μA). Experimentally, its maximum conversion limit is 9 MHz with a maximum current close to 300 μA. Fig. 4F is a zoom of Fig. 4E, showing that the LF converter has a linear behavior for input currents up to 600 nA, which is more than suitable for this application (the photodiode currents do not exceed that value in diffuse reflectance and fluorescence experimental measurements). Finally, it is important to note that, comparing the equations of Fig. 4D and F, the output frequencies for the same input currents are higher in the case of Fig. 4F. For example, for 10 nA, the output frequency obtained with Fig. 4D is 252.7 Hz and with Fig. 4F is 647.8 Hz. This is due to the photodiode total capacitance (that is wavelength dependent, rising with the wavelength), which is not considered in the case of Fig. 4F, where none photodiode was used and the input current was directly injected in the LF input. The higher the photodiode capacitance, the lower is the output frequency. This effect is included, after calibration, for the spectra reconstruction (see Section 3.3). The measured LF converter power consumption was 1 mW, when 3.5 V is applied as power supply [18].

3.2. Diffuse reflectance experimental measurements

Fig. 5 shows the extracted signals for the phantoms presented on Table 1, with the fabricated optical filters and the on-chip photodiode (with 100 μm × 100 μm active area) with and without the respective LF converter, and with a commercial photodiode, for comparison (*Hamamatsu S2386-5 K*). For each measurement, barium sulfate powder, $BaSO_4$ (in a quartz cuvette) was used as reference for the 100% of diffuse reflectance. Moreover, the reflectance of a quartz cuvette with water was subtracted from the total reflectance of each phantom.

As it can be observed in Fig. 5, with the implemented optical setup (Figure S6 of Supplementary Information), it is possible to extract diffuse reflectance signals with very small differences when compared to

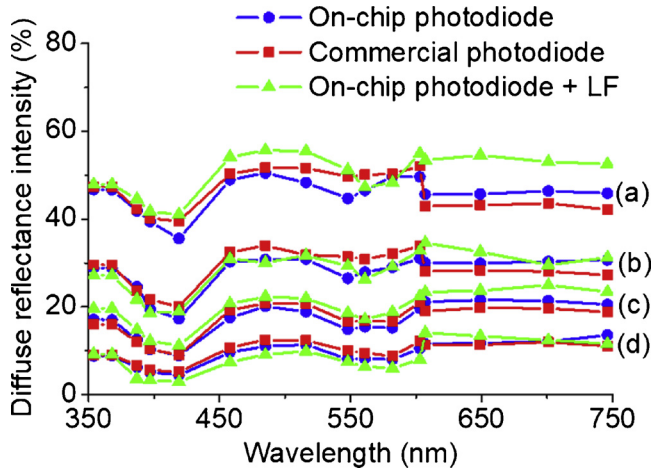

Fig. 5. Diffuse reflectance spectra measured with the optical filters and: one of the photodiodes of the CMOS microsystem (onchip photodiode); the *Hamamatsu S2386-5 K* photodiode (commercial photodiode); and one of the photodiodes of the CMOS microsystem and respective LF converter (on-chip photodiode + LF).

the same signals acquired with a commercial photodiode, proving the viability of the on-chip measurements. Moreover, a similar behavior is observed with all the components assembly (on-chip photodiode + LF), where also the LF converter from the CMOS optical microsystem was used. Concerning the signals behavior, it is in accordance with the expected, with a decrease of the diffuse reflectance signal as hemoglobin (absorber) concentration increases and polystyrene beads (scatterer) concentration decreases (from (a) to (d) on Table 1), both components being the main contributors to the diffuse reflectance signal. Concerning the spectra intensity and shape for all the phantoms, and comparing with the spectra of a similar group of phantoms measured with a commercial spectrophotometer (Table S1 and Figure S8 on section A6 of Supplementary Information), slight differences are noted, especially at wavelengths below 600 nm. In Fig. 5, the spectra intensity values are higher and the second hemoglobin peaks (at 520–590 nm) are not well defined. This may due to some lack of sensitivity of the implemented optical setup. As a result, the effect of hemoglobin in the diffuse reflectance signal is less noted, especially where it must be detected, below 600 nm, because its molar extinction coefficient is higher [21]. However, the typical affectation of hemoglobin in the diffuse reflectance signal is noted especially in its main absorption peaks (350,450 nm and 520–590 nm).

This lack of sensitivity of the optical setup may be due to the distances between the optical elements (Figure S6). In future, this can be reduced with the use of LEDs for illumination, and with deposition of the optical filters on the top of the photodiodes, including the optical filters to remove second order effects of the main optical filters. Nevertheless, it must be emphasized that the hemoglobin concentrations used (Table 1) are always lower than those observed in normal colorectal tissues (around 1.8 mg/mL [22]) showing that this apparatus, as made as a portable small device, is suitable for detecting changes in hemoglobin concentration from normal to dysplastic tissues.

3.3. Fluorescence experimental measurements

Fig. 6A displays the extracted signals for the phantoms presented on Table 2, using one of the CMOS optical microsystem photodiodes (with 100 µm × 100 µm active area), and the fabricated optical filters. It is important to mention that the obtained currents with intensities below 0.023 nA were considered as 0 nA, since this is the limit of the photodiode and readout electronics (dark current, as clarified on Section 3.1). Fig. 6B exhibits the extracted signals with the addition of the respective LF converter. The frequencies below 1 Hz in Fig. 6B are due to the dark current of the photodiode and are background signal that can further be removed by software. For fluorescence measurements, there were used only 12 optical filters (ranging from 368 nm to 607 nm), since that wavelength range covers the fluorescence emission spectra of fluorophores NADH and Carbostyril 124 [23,24].

For diffuse reflectance measurements, it was used a reference ($BaSO_4$ powder) for the 100% of diffuse reflectance, which is very useful because, that way, diffuse reflectance measurements are relative and are not affected by the optical filters transmittance and by the on-chip photodiode efficiency. The same does not happen for fluorescence measurements, being necessary to ensure that the fluorescence signals shape is not affected by the optical filters transmittance and photodiode efficiency. As a result, the same phantoms presented on Table 2 were measured in a commercial spectrofluorometer, using a set of conditions that aims to reproduce the ones of the optical setup presented on Figure S7 of Supplementary Information. The spectra obtained with the commercial equipment are presented on section A7 of Supplementary Information (Table S2 and Figure S9). Comparing the obtained results (Fig. 6A and B) with Figure S9 of Supplementary Information, it can be observed that the shape of the spectroscopic signals is rather similar, with the fluorescence intensity maximum occurring at a wavelength close to 419 nm. However, it could be noted, again, a lack of sensitivity on the optical setup of Figure S7, as the fluorescence signals of phantoms (b) and (c) were not distinguished, unlike it was expected and presented on Figure S9 (Supplementary Information). In spite of this, it can be concluded that the shape of fluorescence signals extracted with the optical setup of Figure S7 is in accordance with the expected, the fluorescence peak occurring at 419 nm and the highest emission intensity corresponding to the phantom with highest fluorophores concentration.

Again, the lack of sensitivity of the optical setup (Figure S7) may be due to the distances between the optical components. In future, it will be crucial to reduce the distances between the elements, as reported at the end of previous section, Section 3.2. Increasing the power of the light source could be a solution for the majority of situations, but in the reported application, it may cause a significant heat of the sample, with a consequent fluorescence quenching, and this effect must be avoided. However, the used concentration of NADH (Table 2) is much lower (in phantom (d) of Table 2 is approximately 113 µg/g) than those reported for normal and malignant oral cavity tissues (above 325 µg/g [25]), highlighting the sensitivity of our microsystem for the desired purposes.

4. Conclusions

This paper reports on-chip experimental diffuse reflectance and fluorescence measurements, performed with an apparatus containing high selective optical filters and a CMOS optical microsystem with photodiodes and LF converters for readout. The microsystem is ready to be used as a portable system on a surgery room. The obtained results using phantoms allow concluding the viability of extracting diffuse reflectance and fluorescence signals with small differences when compared to those obtained with commercial equipment. A lack of sensitivity of the optical setup implemented for spectroscopic measurements was noted, which can be avoided with the reduction of the distance between optical elements, i.e., introducing LEDs for illumination and integrating all the optical filters (even the ones used for eliminate second order effects) on the photodetection system. A promising solution can be the direct deposition, by IBD, of each optical filter on top of the respective photodiode, using a patterned photoresist mask on the CMOS die. With all the optics integrated on a chip, the distances between elements are smaller, allowing a better coupling of light from one element to the next. Moreover, the number of optical interfaces will also be reduced, decreasing the interfaces at which optical losses can occur [26]. A final application of the on-chip spectroscopy microsystem can be its integration within the conventional endoscopes and colonoscopes, to mark possible biopsy sites or even detect early GI cancer

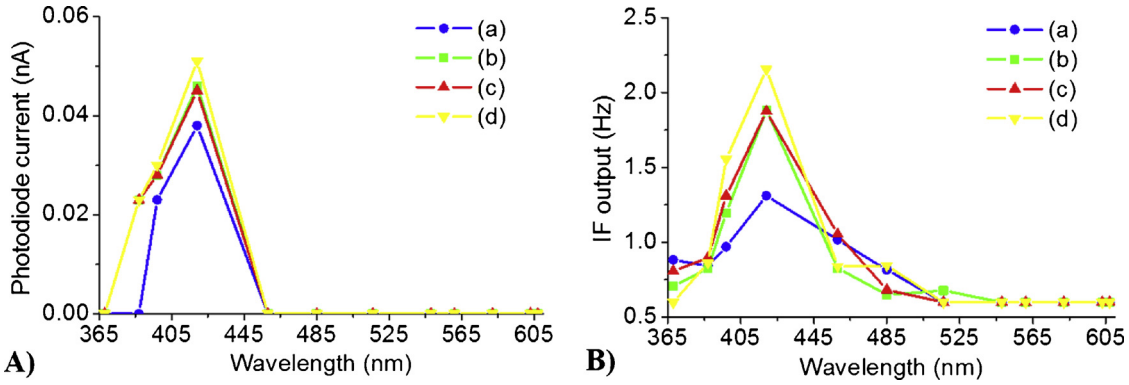

Fig. 6. A) Fluorescence spectra measured with the optical filters and one of the photodiodes of the CMOS microsystem (on-chip photodiode); B) Fluorescence spectra measured adding the respective LF converter.

stages, helping in the therapeutic monitoring.

Acknowledgments

This work was funded by FEDER funds through the "Eixo I do Programa Operacional Fatores de Competitividade" (POFC) QREN, project reference COMPETE: FCOMP-01-0124-FEDER020241 and UID/EEA/04436/2013, COMPETE 2020 with the code POCI-01-0145-FEDER-006941 and by FCT – Fundação para a Ciência e a Tecnologia (Portugal), project reference PTDC/EBB-EBI/120334/2010 and Strategic Funding to CF-UM-UP (UID/FIS/04650/2013). S. Pimenta thanks the FCT for the SFRH/BD/87605/2012 PhD grant. This work is also supported by: project OpticalBrain, PTDC/CTM-REF/28406/2017 operation code NORTE-01-0145-FEDER-028406; project OCT-RAMAN, PTDC/FIS-OTI/28296/2017 operation code NORTE -01-0145-FEDER-028296; and project of Infrastructures Micro&NanoFabs@PT, NORTE-01-0145-FEDER-022090, PORNorte, Portugal 2020.

Appendix A. Supplementary data

Supplementary material related to this article can be found, in the online version, at doi:https://doi.org/10.1016/j.snb.2018.10.142.

References

[1] World Health Organization, Key Factors About Cancer: Fact Sheet Nr. 297, Feb. 2018 (Assessed 20 Mar 2018) http://www.who.int/mediacentre/factsheets/fs297/en/.
[2] S. Pimenta, S. Cardoso, E.M.S. Castanheira, G. Minas, Advances towards a miniaturized optical system for gastrointestinal cancer detection using diffuse reflectance and fluorescence spectroscopies, in: A.K. Tyagi, S. Prasad (Eds.), Gastrointestinal Cancers: Prevention, Detection and Treatment, Nova Publishers, New York, 2016, pp. 313–341.
[3] I. Georgakoudi, B.C. Jacobson, J.V. Dam, V. Backman, M.B. Wallace, M.G. Mueller, Q. Zhang, K. Badizadegan, D. Sun, G.A. Thomas, L.T. Perelman, M.S. Feld, Fluorescence, reflectance, and light scattering spectroscopy for evaluating dysplasia in patients with Barrett's esophagus, Gastroenterology 120 (2001) 1620–1629.
[4] I. Georgakoudi, The color of cancer, J. Lumin. 119-120 (2006) 75–83.
[5] B. Yu, J.Y. Lo, T.F. Kuech, G.M. Palmer, J.E. Bender, N. Ramanujam, Cost-effective diffuse reflectance spectroscopy device for quantifying tissue absorption and scattering in vivo, J. Biomed. Opt. 13 (2008) 060505.
[6] G. Koukouvinos, D. Goustouridis, K. Misiakos, S. Kakabakos, I. Raptis, P. Petrou, Rapid C-reactive protein determination in whole blood with a white light reflectance spectroscopy label-free immunosensor for Point-of-Care applications, Sens. Actuators B Chem. 260 (2018) 282–288.
[7] S. Pimenta, S. Cardoso, A. Miranda, P. De Beule, E.M.S. Castanheira, G. Minas, Design and fabrication of SiO_2/TiO_2 and MgO/TiO_2 based high selective optical filters for diffuse reflectance and fluorescence signals extraction, Biomed. Opt. Express 6 (2015) 3084–3098.
[8] M.G. Müller, I. Georgakoudi, Q. Zhang, J. Wu, M.S. Feld, Intrinsic fluorescence spectroscopy in turbid media: disentangling effects of scattering and absorption, Appl. Opt. 40 (2001) 4633–4646.
[9] J.Q. Brown, K. Vishwanath, G.M. Palmer, N. Ramanujam, Advances in quantitative UV-visible spectroscopy for clinical and pre-clinical application in cancer, Curr. Opin. Biotechnol. 20 (2009) 119–131.
[10] D.S. Ferreira, V.C. Pinto, J.H. Correia, G. Minas, IEEE Trans. Biomed. Eng. 58 (2011) 2633–2639.
[11] D.S. Ferreira, J. Mirkovic, R.F. Wolffenbuttel, J.H. Correia, M.S. Feld, G. Minas, Narrow-band pass filter array for integrated opto-electronic spectroscopy detectors to assess esophageal tissue, Biomed. Opt. Express 2 (2011) 1703–1716.
[12] Q.-S. Wan, T. Wang, K.-H. Zhang, Biomedical optical spectroscopy for the early diagnosis of gastrointestinal neoplasms, Tumor Biol. 39 (2017) 1010428317717984 (12 pages).
[13] J.Y. Lo, B. Yu, H.L. Fu, J.E. Bender, G.M. Palmer, T.F. Kuech, N. Ramaimjam, A strategy for quantitative spectral imaging of tissue absorption and scattering using light emitting diodes and photodiodes, Opt. Express 17 (2009) 1372–1384.
[14] B. Sciacca, A. Franc, P. Hoffmann, T.M. Monro, Multiplexing of radiative-surface plasmon resonance for the detection of gastric cancer biomarkers in a single optical fiber, Sens. Actuators B 183 (2013) 454–458.
[15] K. Imaizumi, Y. Harada, N. Wakabayashi, Y. Yamaoka, H. Konishi, P. Dai, H. Tanaka, T. Takamatsu, Gastrointest. Endosc. 75 (2012) 110–117.
[16] D. Liu, X. Zhao, X. Zeng, H. Dan, Q. Chen, Non-invasive techniques for detection and diagnosis of oral potentially malignant disorders, Tohoku J. Exp. Med. 238 (2016) 165–177.
[17] L.Y. Robles, S. Singh, P.M. Fisichella, Emerging enhanced imaging technologies of the esophagus: spectroscopy, confocal laser endomicroscopy, and optical coherence tomography, J. Surg. Res. 195 (2015) 502–514.
[18] R.G. Correia, S. Pimenta, G. Minas, CMOS integrated photodetectors and light-to-frequency converters for spectrophotometric measurements, IEEE Sensors J. 17 (2017) 3438–3445.
[19] O. Schmidt, P. Kiesel, M. Bassler, Performance of chip-size wavelength detectors, Opt. Express 15 (2007) 9701–9706.
[20] Y. Wan, J.A. Carlson, S.A. Al-Mulla, W. Peng, K.D. Long, B.A. Kesler, P. Su, J.M. Dallesasse, B.T. Cunningham, Integrated spectroscopic analysis system with low vertical height for measuring liquid or solid assays, Sens. Actuators B 255 (2018) 935–943.
[21] S. Prahl, Optical Absorption of Hemoglobin, Available at: (1999) (Accessed February, 2018), http://omlc.org/spectra/hemoglobin/.
[22] H.W. Wang, J.K. Jiang, C.H. Lin, J.K. Lin, G.J. Huang, J.S. Yu, Diffuse reflectance spectroscopy detects increased hemoglobin concentration and decreased oxygenation during colon carcinogenesis from normal to malignant tumors, Opt. Express 17 (2009) 2805–2817.
[23] X. Dai, E. Rollin, A. Bellerive, C. Hargrove, D. Sinclair, C. Mifflin, F. Zhang, Wavelength shifters for water Cherenkov detectors, Nucl. Instrum. Methods Phys. Res. A 589 (2008) 290–295.
[24] Sigma-Aldrich, Product Information - Beta-Nicotinamide adenine dinucleotide, reduced disodium salt hydrate. Available at: http://www.sigmaaldrich.com/content/dam/sigma-aldrich/docs/Sigma/Product_Information_Sheet/2/n6005pis.pdf (accessed February, 2016).
[25] A. Uppal, P.K. Gupta, Measurement of NADH concentration in normal and malignant human tissues from breast and oral cavity, Biotechnol. Appl. Biochem. 37 (2003) 45–50.
[26] G. Minas, S.O. Catarino, Lab-on-a-chip devices for chemical analysis, in: D. Li (Ed.), Encyclopedia of Microfluidics and Nanofluidics, Springer, New York, 2015, pp. 1511–1531.